Supplementary Material for: THz response and colossal Kerr rotation from the surface states of the topological insulator Bi_2Se_3

R. Valdés Aguilar,[1,*] A.V. Stier,[1,2] W. Liu,[1] L.S. Bilbro,[1] D.K. George,[2] N. Bansal,[3] L. Wu,[1] J. Cerne,[2] A.G. Markelz,[2] S. Oh,[3] and N.P. Armitage[1,†]

[1] *The Institute for Quantum Matter, Department of Physics and Astronomy, The Johns Hopkins University, Baltimore, MD 21218 USA.*

[2] *Department of Physics, University at Buffalo. State University of New York. Buffalo, NY 14260*

[3] *Department of Physics and Astronomy, Rutgers the State University of New Jersey. Piscataway, NJ 08854*

Film growth.

Thin films of topological insulator Bi_2Se_3 of varied thicknesses were grown at Rutgers by a molecular beam epitaxy (MBE) technique on 0.5 mm thick sapphire substrates (Al_2O_3). Films were grown on ozone-cleaned surfaces using the two-temperature growth process. Evolution of the film surface during growth was monitored by RHEED. After deposition of 3 QL of Bi_2Se_3 at 110° C, a sharp streaky pattern was observed, indicating the growth of single-crystal Bi_2Se_3 structure. The film was then slowly annealed to a temperature of 220° C, which helped further crystallization of the film as seen by the brightening of the specular spot. The diffraction pattern and the Kikuchi lines became increasingly sharp on further deposition. This shows that the grown films have atomically flat morphology and high crystallinity. This process led to high quality single crystalline films with the largest terraces, highest bulk mobilities, and lowest volume carrier densities as detailed elsewhere [1].

THz Methods

TDTS measurements in zero magnetic field were performed at JHU using a home-built transmission based time-domain THz spectrometer. In this technique, an infrared femtosecond laser pulse is split into two paths and sequentially excite a pair of photoconductive 'Auston'-switch antennae on radiation damaged silicon on sapphire. A broadband THz range pulse is emitted by one antenna, transmitted through the Bi_2Se_3 film, and measured at the other antenna. By varying the length-difference of the two paths, the electric field of the transmitted pulse is measured as a function of time. Ratioing the Fourier transform of the transmission through the Bi_2Se_3 film on a substrate to that of a bare reference substrate we resolve the frequency dependent complex transmission of the film. The transmission is inverted to obtain the complex conductance by the standard formula for thin films on a substrate: $\tilde{T}(\omega) = [(1+n)/(1+n+Z_0\tilde{G}(\omega))]e^{i\Phi_s}$ where Φ_s is the phase accumulated from the small difference in thickness between the sample and reference substrates, n is the substrate index of refraction, $Z_0 \approx 377\ \Omega$ is the vacuum impedance, and $\tilde{G} = G_{xx}^{'} + iG_{xx}^{''}$ is the film's effective complex conductance. In the case of topological insulators, the effective conductance is composed of a sum of a bulk contribution, $\tilde{G}_{bulk}=\sigma_{bulk} \times t$ where t is the film thickness, and a surface contribution $2\tilde{G}_{surface}$.

It has recently been discovered that the transport characteristics of this thin films depend on time exposed to different ambient conditions [2]. A similar effect has been discovered in the terahertz response. All measurements reported in this work were performed at least 2 weeks after the film's growth. In the intervening time the thin films were stored in a low humidity environment with relative humidity values of less than ∼15%. The terahertz study of this effects will be reported elsewhere, but we note that, together with the DC study [2], we can speculate that the bulk mobility and carrier density change with exposure time.

Experiments in magnetic field were done in a similar fashion via TDTS spectroscopy at UB. The detection of THz radiation in this system is achieved by electro-optic means. In this method a ZnTe crystal is impinged upon by a part of the infrared femtosecond laser; when the THz pulse reaches the ZnTe crystal, it becomes birefringent and changes the polarization characteristics of the infrared beam. The changes in the polarization of the infrared ultrafast laser beam, which are proportional to the THz electric field strength, are measured by balanced photodiode detection.

As shown in Fig 1c, measurements in field were done in two configurations using three wire grid polarizers of THz radiation (P1, P2 and P3). P1 was placed before the sample to ensure linearly polarized light was incident to the film, P2 and P3 were placed after the sample where P2 was placed in a standard rotating holder that allowed the selection of the polarizer angle (ϕ). In the first setup we measured the transmitted amplitude as a function of P2's angle ϕ, with polarizers P1 and P3 parallel to each other at 0 degrees (collinear configuration). In this mode, we expect the

amplitude of the electric field to have the dependence on ϕ as $|\cos(\phi-\varphi)\cos(\phi)|$, where φ is the pulse rotation angle measured with respect to the position of the first polarizer. In the second configuration, P1 and P3 are perpendicular to each other, at 45° and -45° from the vertical (cross polarizer configuration), and again we measure the intensity as a function of ϕ. In this case the amplitude of the electric field should have an angle dependence as $|\cos(\phi-\varphi)\sin(\phi)|$. In the cross polarizer configuration, the first polarizer had an angle of 45° with respect to the collinear configuration due to the sensitivity of the electro-optic detection to the polarization of the pulse.

The third experimental configuration used for complete characterization of the Kerr angle in the frequency-magnetic field plane was done using a polarization modulation technique. P2 was held in a fast rotating stage and was placed between P1 and the sample, with polarizers P1 and P3 both collinear and oriented vertically (0°). The fast rotator is spun at approximately 600 rpm, and the resulting signal is demodulated by a lockin amplifier at twice the frequency set by the rotation speed. In such an experiment the in-phase signal of the lock-in is proportional to the transmitted electric field collinear with the incoming polarization (X signal), and the out-of-phase response is proportional to the electric field at 90° from the original polarization (Y signal) [3–5]. This method allows fast magnetic field scanning and the analysis of the full spectral response. The X and Y time dependent signals are Fourier transformed to obtain $\tilde{X}(\omega)$ and $\tilde{Y}(\omega)$. By taking the ratio of $\tilde{Y}(\omega)$ to $\tilde{X}(\omega)$, we obtain the tangent of the rotation angle as $\tan[\varphi(\omega)]=\frac{\tilde{Y}(\omega)}{\tilde{X}(\omega)}$. In this work we plot the absolute value of φ.

Temperature dependent conductance.

We fit the zero field THz conductance data using a 2D model dielectric constant consisting of two identical Drude terms for the free electron response, a Drude-Lorentz oscillator for the phonon, and a dielectric constant (ε_∞) that represents the high frequency optical transitions, $\varepsilon_{xx} = 1 + \frac{4\pi i\sigma_{xx}}{\omega}$, where $\sigma_{xx} = \mathrm{G}_{xx}/t$ with t the film thickness:

$$\varepsilon_{xx} = \varepsilon_\infty - \frac{\omega_{pD}^2}{\omega^2 - i\omega\Gamma_D} + \frac{\omega_{pP}^2}{\omega_P^2 - \omega^2 - i\omega\Gamma_P} \tag{S1}$$

Here the subscripts D and P represent the Drude and the phonon contributions, respectively. We measured 4 samples of thicknesses 16, 32, 64 and 100 QL (1 QL $\sim$ 0.94 nm) in the temperature range between 2 and 300 K. Fig. S1 shows the real and imaginary conductances at several temperatures for the 100QL sample. The fit parameters are given in Table 1, where the spectral weight for the Drude term contains the contribution from both surfaces.

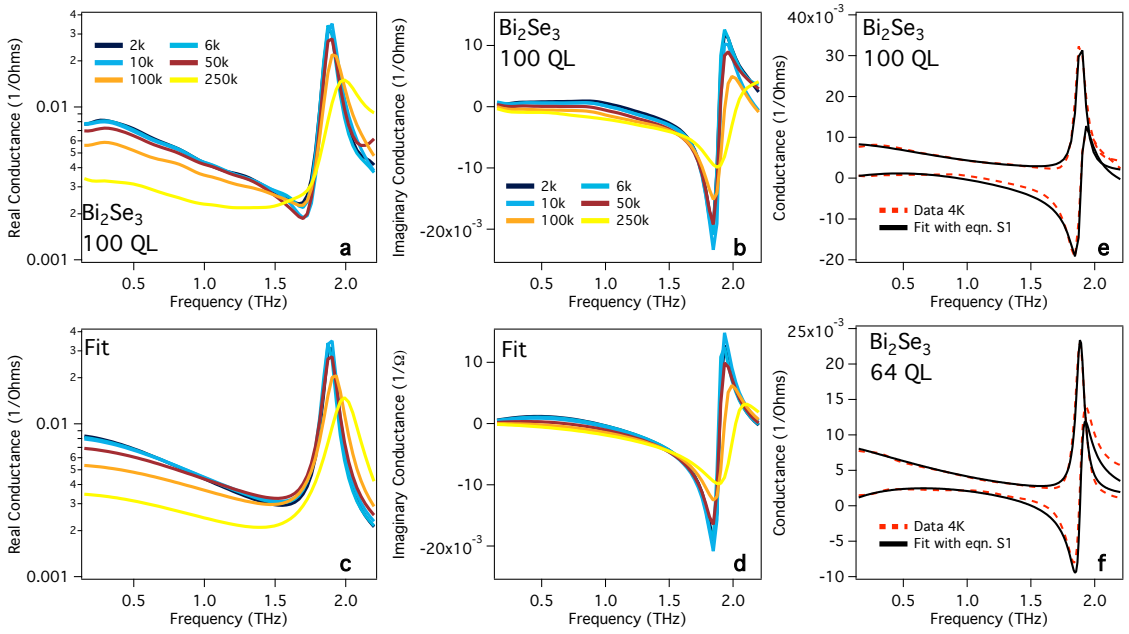

FIG. S1: Frequency and temperature dependent conductance. **a**). Measured real and **b**) imaginary conductances for the 100 QL sample for the displayed temperatures. **c**) and **d**). Respective fits using the model described in equation S1. **e**) and **f**). Overlay of fits with data for 100 and 64 QL thicknesses.

TABLE I: Fitting parameters for the Drude and phonon contributions to the conductance at zero field and 6 K.

	$(\omega_{pD}/2\pi)^2\times$ t (THz$^2\times$nm)	$\gamma_D=\Gamma_D/2\pi$ (THz)	$(\omega_{pP}/2\pi)^2\times$ t (THz$^2\times$nm)	$\omega_P/2\pi$ (THz)	$\gamma_P=\Gamma_P/2\pi$ (THz)	$\varepsilon_\infty\times$ t (nm)
16QL	193,382	1.41	4,067	1.89	0.108	38,592
32QL	201,014	1.37	14,440	1.92	0.094	103,793
64QL	148,818	1.01	35,867	1.89	0.081	19,664
100QL	157,253	1.02	53,124	1.90	0.086	61,975

Calculation of Kerr angle for a thin metallic film.

The Faraday (ϕ_F) and Kerr (ϕ_K) angles are defined as:

$$\tan(\varphi_F)=i\frac{t_+-t_-}{t_++t_-}$$
$$\tan(\varphi_K)=i\frac{r_+-r_-}{r_++r_-}$$

where $t_\pm$ ($r_\pm$) is the transmission (reflection) coefficient for (+) right circularly polarized and (-) left circularly polarized light. In the case of the wavelength of light being much larger than the thickness of the film, we obtain the reflection and transmission coefficients as follows.

$$r_\pm=\frac{n-1-Z_0\mathrm{G}_\pm}{n+1+Z_0\mathrm{G}_\pm}$$
$$t_\pm=\frac{2}{n+1+Z_0\mathrm{G}_\pm}$$

where $\mathrm{G}_\pm=\mathrm{G}_{xx}\pm i\mathrm{G}_{xy}$ are the (+) right and (-) left circularly polarized conductances. The conductances have the usual form for the free carrier response in a magnetic field as follows:

$$\mathrm{G}_{xx}=\frac{\omega_{pD}^2/(4\pi)(\Gamma-i\omega)}{(\Gamma-i\omega)^2-\omega_c^2}$$
$$\mathrm{G}_{xy}=-\frac{\omega_{pD}^2/(4\pi)\omega_c}{(\Gamma-i\omega)^2-\omega_c^2}$$

where $\omega_c=e\mathbf{B}/m^*c$ is the cyclotron frequency.

We can then simplify for the Kerr angle when reflection happens *within* the substrate, i.e. at the substrate-TI interface, as:

$$\tan(\varphi_K)=\frac{2nZ_0\mathrm{G}_{xy}}{n^2-1-2Z_0\mathrm{G}_{xx}-Z_0^2(\mathrm{G}_{xx}^2+\mathrm{G}_{xy}^2)} \tag{S2}$$

Similarly, the Kerr angle can be calculated for the case of reflection from the vacuum-TI interface:

$$\tan(\varphi_K)'=\frac{2Z_0\mathrm{G}_{xy}}{1-n^2-2nZ_0\mathrm{G}_{xx}-Z_0^2(\mathrm{G}_{xx}^2+\mathrm{G}_{xy}^2)} \tag{S3}$$

We note that among the differences between equations S2 and S3 are the appearance of the substrate's index of refraction n in the numerator, which makes the rotation larger by this factor, as well as its multiplication in the denominator of the factor $-2nZ_0\mathrm{G}_{xx}$ in eqn. S3 which makes its rotation smaller (by making the denominator larger). In the quantum Hall effect regime that is relevant for the topological magnetoelectric effect ($\mathrm{G}_{xx}\sim 0$ and $\mathrm{G}_{xy}\sim e^2/h$) these expressions can be simplified to:

$$\tan(\varphi_K)\sim\frac{2nZ_0\mathrm{G}_{xy}}{n^2-1}=\frac{n\alpha}{n^2-1}$$
$$\tan(\varphi_K)'\sim\frac{2Z_0\mathrm{G}_{xy}}{1-n^2}=\frac{\alpha}{1-n^2}$$

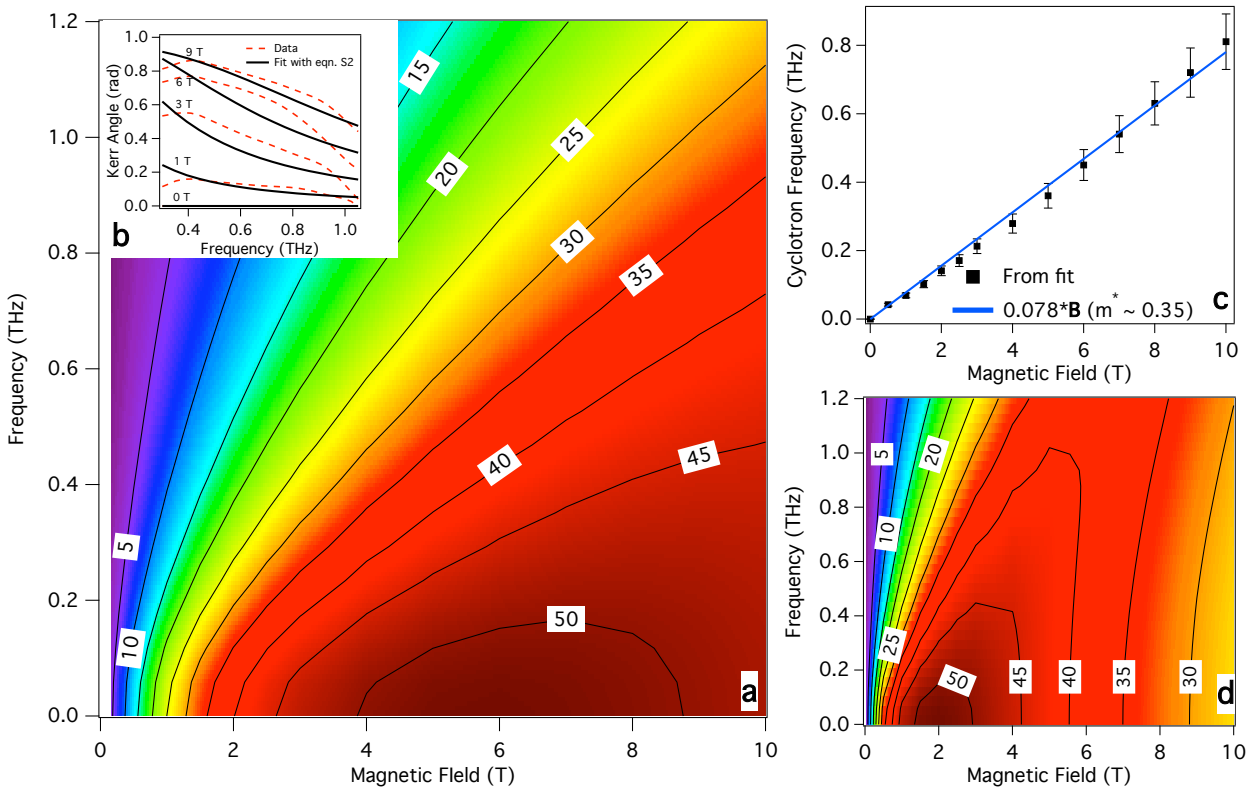

FIG. S2: Calculation of Kerr angle and cyclotron frequency. **a)** Calculated absolute value of the Kerr angle ($|\varphi_K|$) as a function of frequency and magnetic field using the parameters given in the text. **b)** Representative fits using eqn. S2 to the magnitude of the Kerr angle. **c)** Cyclotron frequency obtained from fitting the low frequency part of the spectrum (symbols), line is obtained by taking the effective mass $m^* \sim 0.35$ m_e. **d** Calculation of the Kerr angle for an effective mass of $m^* \sim 0.12$ m_e.

where α is the vacuum fine structure constant. Thus, it is clear that making the reflection measurement from *within* the substrate leads to an enhancement of the Kerr angle by the substrate's index of refraction.

With equation S2 we can reproduce the magnitude, frequency and field dependence of the measured Kerr angle (Fig. S2(a)) with an almost linear dependence of the cyclotron frequency on magnetic field (Fig. S2(c)). The effective mass $m^* \sim 0.35$ m_e is obtained from the cyclotron frequency. Figure S2(b) shows representative fits to the Kerr angle as function of frequency for different magnetic field values using equation S2. As discussed in the main text, taking an effective mass of 0.12 m_e, which is the one obtained for the states induced by band-bending near the surface [6], one cannot reproduce the results of the experiment as shown in Fig. S2(c). Similarly poor comparison with the data can be obtained when the bulk effective mass, $m^* \sim 0.16$ m_e, is used.

* Electronic address: rvaldes@pha.jhu.edu
† Electronic address: npa@pha.jhu.edu

[1] N. Bansal, Y. Kim, M. Brahlek, E. Edrey, and S. Oh (2011), arxiv:1104.5709.
[2] M. Brahlek, Y. Kim, N. Bansal, E. Edrey, and S. Oh, Appl. Phys. Lett. **99**, 012109 (2011).
[3] M. Grayson, L. B. Rigal, D. C. Schmadel, H. D. Drew, and P.-J. Kung, Phys. Rev. Lett. **89**, 037003 (2002).
[4] P.P. Markowicz, M. Samoc, J. Cerne, P.N. Prasad, A. Pucci, and G. Ruggeri, Opt. Exp. **12**, 5209 (2004).
[5] G. S. Jenkins, D. C. Schmadel, and H. D. Drew, Review of Scientific Instruments **81**, 083903 (2010), ISSN 10897623.
[6] P. D. C. King, R. C. Hatch, M. Bianchi, R. Ovsyannikov, C. Lupulescu, G. Landolt, B. Slomski, J. H. Dil, D. Guan, J. L. Mi, et al., Phys. Rev. Lett. **107**, 096802 (2011).